Performing Energy-Efficient Pick-and-Place Motions for High-Speed Robots by using Variable Stiffness Springs

Rafael Balderas Hill, Sébastien Briot, Abdelhamid Chriette, Philippe Martinet

Performing Energy-Efficient Pick-and-Place Motions for High-Speed Robots by using Variable Stiffness Springs

Rafael Balderas Hill [†‡], Sébastien Briot [‡§*], Abdelhamid Chriette [†‡], and Philippe Martinet [¶]

[†] Ecole Centrale de Nantes, 44321 Nantes, France
[‡] Laboratoire des Sciences du Numérique de Nantes (LS2N), UMR CNRS 6004, 44321 Nantes, France
[§] Centre National de la Recherche Scientifique (CNRS)
[¶] Centre de Recherche Inria Sophia Antipolis, 06902 Sophia Antipolis, France
Email: {Rafael.Balderashill, Sebastien.Briot, Abdelhamid.Chriette}@ls2n.fr, Philippe.Martinet@inria.fr
[*] Corresponding author

Typically, for pick-and-place robots operating at high speeds, an enormous amount of energy is lost during the robot braking phase. This is due to the fact that, during such operational phase, most of the energy is dissipated as heat on the braking resistances of the motor drivers. In order to increase the energy-efficiency during the high-speed pick-and-place cycles, this paper investigates the use of variable stiffness springs (VSS) in parallel configuration with the motors. These springs store the energy during the braking phase, instead of dissipating it. The energy is then released to actuate the robot in a next displacement phase. This design approach is combined with a motion generator which seeks to optimize trajectories for input torques reduction (and thus of energy consumption), through solving a boundary value problem (BVP) based on the robot dynamics. Experimental results of the suggested approach on a five-bar mechanism show the drastic reduction of input torques, and therefore of energetic losses.

1 Introduction

It is known that one of the most representative challenges in industrial robotics is to increase the energy efficiency of robot manipulators. Typically, in industrial applications, such as high-speed pick-and-place operations, accuracy while picking and placing objects in the robot workspace is the most important criteria to evaluate the robot performance [1]. Nonetheless, the design trends of pick-and-place robots operating at high speeds have shifted to the design of robots that in addition to be accurate [2], they can perform as energy-efficient as possible [1]. The motivations to do that rely on the environmental impacts associated to the energy consumption when performing high-speed motions. This is due to the fact that powerful motor drive systems are required to attain the power specifications of moving the robot structure at high speeds, thus increasing the energetic consumption [3]. Additionally, due to a continuous increase of the electricity cost, finding new ways to reduce the energy consumption has become crucial in the recent years.

The most common strategies to reduce the energy consumption at high speeds consist either on optimizing the robot trajectory [4] or in designing lightweight robot architectures, e.g. by using carbon fiber for lowering the mass of the moving elements, thus permitting the use of less powerful motors [5]. Nevertheless, designing a lightweight robot structure may affect the robot stiffness, which would negatively impact the accuracy of the robot at high speeds. Another approach for the reduction of the energy consumption was presented in [6–8] in which it has been shown that, by using gravity-balancing techniques, it is possible to compensate the input efforts to move slow pick-and-place robots, thus reducing the energy consumed at slow speeds. Nevertheless, since at high speeds the inertial effects become preponderant with respect to the other dynamic terms, these techniques cannot be applied.

Thus, another approach to cope with the energy storage issues is the use of compliant actuators, such as the series elastic actuators (SEAs) [9], the variable stiffness actuators (VSAs) [10–13], and the most recent ones the series-parallel elastic actuators (SPEAs) [14, 15]. The SEAs are compliant actuators that decouple the motor and the output load by means of a spring in series that serves as energy storage, and whose stiffness is set by the spring constant. Even if the SEAs have shown their effectiveness in applications to absorb impacts and to ensure safety, such as in humanoid robots [16] and in human-robot interaction [17], respectively, their main limitation is that the fixed stiffness restrict the level of compliance to adapt for different tasks. Therefore, the VSAs were introduced to overcome the limitations of the SEAs, and to handle with the energy storage issues. VSAs

decouple the motor and the output load by a spring in series, whose stiffness can be controlled. Such actuators have been recently introduced to considerably reduce the energy consumption of pick-and-place robots in [18]. Nevertheless, the main issue is that the serial arrangement of springs and motors in the VSAs would lead to uncontrolled deflections, worsening the accuracy of the robot end-effector when performing pick-and-place motions at high speeds.

The SPEA [14, 15] is a new type of actuator for lowering the input efforts, and thus the energy consumption. It is an actuator that consists of a single motor that deforms a sequence of several parallel elastic elements, in which a gear system serves as intermittent mechanism to couple and decouple the springs in the parallel arrangement. Even if such type of actuator allows to vary the stiffness to adapt to different specified tasks, its design complexity results of low practicability to perform high-speed motions due to the reaction time to lock and unlock the intermittent mechanism.

A novel type of actuation for pick-and-place robots in [19–24] proposes the use of constant stiffness springs in parallel to the motors in order to minimize the input efforts from the actuators while ensuring accuracy. This is possible due to the stored potential energy that the spring in parallel is able to supply so that the output load moves, thus reducing the torque demanding from the main motor. Even if the results are impressive, the level of compliance, and thus of adaptation for different travel times and amplitudes, is limited by the spring constant.

In order to overcome the limitations in terms of adaptability of the constant stiffness springs placed in parallel, the authors in [25, 26] proposed to use an additional motor to vary the stiffness of the springs placed in parallel to the motors that actuate the joints. These springs are called variable stiffness springs[1] (VSS) [27]. This was applied to a slow robot manipulator. To the best of our knowledge, the authors in [25], were the first on introducing the concept of using variable stiffness springs (VSS) in parallel to the motors for improving the adaptability to quasi-periodic tasks for slow pick-and-place robots. The work in [26] proposes a control-based approach by means of a VSS elasticity adaptation law, in which the output stiffness of the VSS can be controlled by means of a nonlinear force/displacement relation for the springs. Even if the results are impressive with a reduction of 72 % for slow pick-and-place motions, among several drawbacks, which makes difficult to conclude which is the real energy gain, we can list: *i*) the friction is neglected, *ii*) the energy required to adjust the VSS is not considered when analyzing the percentages of energy savings, and *iii*) the cycle times used for the experiments are of 13 s, far from a typical high-speed cycle time; *iv*) Finally, since the approach in [26] proposes to use a stiffness-based control approach, i.e. to generate stiffness profiles (instead of spring equilibrium position trajectories), it is thus necessary to estimate the VSS stiffness in the control loop, which complexifies the control system due to the requirement of measuring the stiffness in the feedback.

Recently, the authors of the present paper have shown in [28, 29] the effectiveness of using VSS in parallel for noticeably increasing the energy efficiency of pick-and-place robots operating at high speeds. Additionally, it has been shown that the energy required to adjust the spring equilibrium position of the VSS (associated to the VSS stiffness) is not negligible when analyzing the energetic losses in the full actuation chain. Regarding the strategies for energy savings in [28, 29], firstly, the work in [28] seeks to exploit an energetic model that groups the losses in the full actuation chain of the parallel robot with VSS, by generating trajectories through an optimization formulation. Even if it is shown that the energy efficiency can be increased by 48 %, the motions used in the optimization are polynomial-based trajectories that do not fully exploit the robot natural dynamics leading to the convergence towards a local minima of the energetic criteria. Additionally, only simulation results are presented. Since a pick-and-place operation is described by quasi-periodic oscillatory motions, through the addition of the VSS it should be possible to exploit such quasi-oscillations in order to match the free-response of the system with the desired pick-and-place motions. Therefore, the work in [29] presents a strategy to generate energy-efficient motions by adjusting the spring equilibrium positions of the VSS in parallel so that the robot pseudo-periodic pick-and-place oscillations match the system free-response. This strategy permits to reduce the input efforts of the robot active joints, and therefore the energy consumed by the actuators by 50 %. Nonetheless, since the efforts required to actuate the VSS are not optimized, they become preponderant with respect to the main robot active joint torques when analyzing the full actuation chain energy savings, i.e. robot-plus-VSS. Moreover, the work in [29], presents only simulation results, which makes difficult to estimate in real operating conditions, which are the energy savings.

In this paper, we consider the problem of exploiting the combined motion of robot and VSS joints in the same time, thus minimizing the overall energy consumption of the robot plus the VSS simultaneously, which was never done before. This is achieved thanks to the formulation of a boundary value problem (BVP) in which both the parallel robot and VSS dynamic equations are coupled and solved for the desired boundary pick-and-place conditions, thus generating natural motions considering the combined robot-plus-VSS natural dynamics.

This paper is thus structured as follows: Section 2 presents the dynamic modeling of robots and VSS. Section 3 shows the BVP formulation for generating energy-efficient pick-and-place trajectories considering the robot and VSS dynamics simultaneously. Section 4 presents the results of the proposed approach on an industrial-sized five-bar mechanism with VSS in parallel to the actuated links. Furthermore, in order to show the effectiveness of the suggested actuation chain, two types of actuation are compared: i) nominal actuation, which consists of the parallel robot without springs; ii) use of VSS in parallel with the robot actuated links.

[1]The terminology "variable stiffness spring" is ambiguous: Indeed, this is not the stiffness of the springs that is changing but their attachment points. However, this terminology being often used in the literature, we preferred to keep it unchanged.

2 Dynamic analysis of the parallel configuration of VSS and motors

2.1 Actuation concept based on VSS in parallel

In order to increase the energy efficiency while ensuring accuracy when performing high-speed pick-and-place operations, the purpose of this work is to present a strategy to dynamically exploiting the actuation principle based on VSS. As explained earlier, the springs will be used as energy storage devices: during the deceleration phase, they will store the robot energy, thus avoiding to release it on the electrical network and dissipate it by heat; during the acceleration phase, the energy stored in the springs will be released to the mechanical system, thus reducing the necessity to provide current to the motors in order to put the robot into motion. VSS being springs whose anchor points could be controlled, it is possible to adapt their stiffness such that the robot is able to reduce its energy consumption for a large range of motions.

Let us first describe the modified robot with VSS. It should be mentioned that the robots considered in the present paper are of parallel architecture. This is because many high-speed pick-and-place industrial robots are parallel robots. However, the presented energy-consumption strategy could be applied other types of robot manipulators.

According to Fig. 1, we will consider a general parallel manipulator with torsional VSS in parallel with the robot motors. The architecture is composed of a rigid fixed base, which is attached to the global frame $\mathcal{F}_0(O,\mathbf{x}_0,\mathbf{y}_0,\mathbf{z}_0)$, a rigid moving platform, attached to $\mathcal{F}_p(\mathcal{P},\mathbf{x}_p,\mathbf{y}_p,\mathbf{z}_p)$, and n active joint variables (n corresponding as well to the number of legs). For the variable stiffness system, we will consider n_s variable stiffness springs. It is worth noticing that, as depicted in Fig. 2, the variable stiffness springs are placed in parallel to the robot actuated links, thus ensuring direct power connection between motors and links of the robot.

The parameterization of the different bodies of the kinematic architecture Fig. 1 is defined as follows:

- $\mathcal{P}$ represents the moving platform;
- $\mathcal{M}_i$ represents the motor that actuate the ith leg of the parallel robot,
- $\mathcal{M}_{s_i}$ represents the motor that actuate the ith variable stiffness spring,

for $i = 1,...,n$.

2.2 Recalls on the dynamic modeling of parallel robots

In order to compute the dynamic model of parallel robots with VSS in parallel, we will firstly compute the dynamic model of the parallel robot alone.

Let us thus briefly recall the formulation for computing the dynamic model of parallel robots presented in [30]. We will consider a parallel robot composed of n degrees of freedom and driven by n active joints. The links are considered to be rigid. Moreover, friction is taken into account in the joints by using the linear model proposed in [31]. The position and velocity of the parallel robot can be described as: $\mathbf{q}$ and $\dot{\mathbf{q}}$ representing the n-dimensional vectors of active joint variables and of active joint velocities, respectively. $\mathbf{x}$ and $\dot{\mathbf{x}}$ will represent the n-dimensional vectors of platform pose and of its time derivatives, respectively. The input-output kinematic constraint that describes the relation between $\dot{\mathbf{x}}$ and the active joint velocities $\dot{\mathbf{q}}$ is given by:

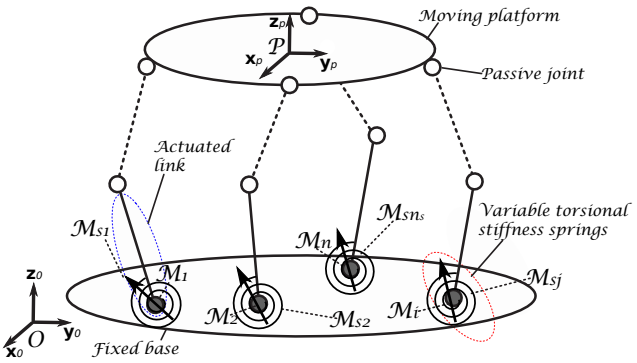

Fig. 1. A general parallel robot with variable stiffness torsional springs in parallel configuration with the actuated links.

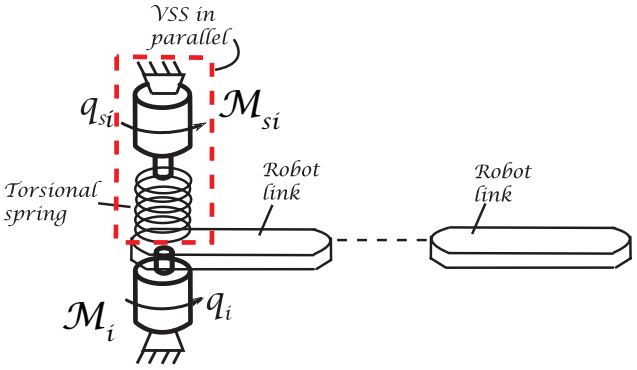

Fig. 2. Power transmission system of variable stiffness springs in parallel to the motors. q_i and q_{s_j} represent the parallel robot joints and variable stiffness joints coordinates, respectively, and $i = 1,...,n$, $j = 1,...,n_s$.

$$\mathbf{A}\dot{\mathbf{x}} + \mathbf{B}\dot{\mathbf{q}} = \mathbf{0} \tag{1}$$

where $\mathbf{A}$ and $\mathbf{B}$ are the $(n \times n)$ parallel and serial kinematic Jacobian matrices, respectively [32]. Then, by using the Lagrange formalism, the dynamic model of the robot can be written as follows:

$$\boldsymbol{\tau} = \boldsymbol{\tau}_{ta} - \mathbf{B}^T\boldsymbol{\lambda}, \qquad \mathbf{w}_p = \mathbf{A}^T\boldsymbol{\lambda} \tag{2}$$

where $\boldsymbol{\tau}$ is the n-dimensional vector of the robot input efforts, $\boldsymbol{\lambda}$ is the n-dimensional vector of Lagrange multipliers, $\boldsymbol{\tau}_{ta}$ and $\mathbf{w}_p$ are the n-dimensional vectors defined by:

$$\boldsymbol{\tau}_{ta} = \frac{\mathrm{d}}{\mathrm{d}t}\left(\frac{\partial L}{\partial \dot{\mathbf{q}}}\right)^T - \left(\frac{\partial L}{\partial \mathbf{q}}\right)^T, \mathbf{w}_p = \frac{\mathrm{d}}{\mathrm{d}t}\left(\frac{\partial L}{\partial \dot{\mathbf{x}}}\right)^T - \left(\frac{\partial L}{\partial \mathbf{x}}\right)^T \tag{3}$$

where L is the Lagrangian of the parallel robot without the VSS.

From equations in (2), considering matrix $\mathbf{A}$ to be full rank, i.e. out of Type 2 singularity [33], the dynamic model of a parallel robot can be obtained as:

$$\boldsymbol{\tau} = \boldsymbol{\tau}_{ta} - \mathbf{B}^T\mathbf{A}^{-T}\mathbf{w}_p \tag{4}$$

which, according to [30], can be written in its decoupled form:

$$\boldsymbol{\tau} = \mathbf{M}\ddot{\mathbf{q}} + \mathbf{c} + \mathbf{f}_a \tag{5}$$

where $\mathbf{M}$ is an $(n \times n)$ definite positive matrix of inertia depending on the active joints coordinates $\mathbf{q}$ and platform coordinates $\mathbf{x}$. $\mathbf{c}$ is an n-dimensional vector of Coriolis, centrifugal and gravitational effects and its value depends on the robot configuration and velocity. $\mathbf{f}_a$ is an n-dimensional vector grouping the active joint friction terms.

2.3 Modeling of the robot plus the VSS in parallel with the actuated links

Before developing the dynamic modeling of the VSS, it is worth mentioning that here we will only consider torsional springs for the VSS. This is done due the fact that, as it will be shown in Section 4, the experimental benchmark is composed of only revolute joints. Thus, since pure torsional springs are deformed with only the application of torques (same for actuating revolute joints), the VSS actuation would be more motion-natural by using torsional springs in the full actuation chain (See Fig. 2). However, the approach could also be extended to linear springs.

In what follows, for the dynamic model of the VSS, we will refer to $\mathbf{q}_s$ and $\dot{\mathbf{q}}_s$ as the n-dimensional vectors of variable stiffness joint variables and velocities, respectively. By considering the effects of the elastic deformation of the springs (due to q_i and q_{s_j}) with their force/displacement relations, the dynamics in (5) become:

$$\boldsymbol{\tau} = \mathbf{M}\ddot{\mathbf{q}} + \mathbf{c}(\mathbf{q}, \dot{\mathbf{q}}) + \mathbf{f}_a + \boldsymbol{\tau}_s \tag{6}$$

where $\boldsymbol{\tau}_s$ is the n-dimensional vector of elastic torques associated to the VSS coupled to the robot in parallel, and whose analytic expression follows from the Lagrange formalism:

$$\boldsymbol{\tau}_s = \mathbf{K}(\mathbf{q} - \mathbf{q}_s) \tag{7}$$

where $\mathbf{K}$ is the $(n \times n)$ stiffness matrix, and the dynamics of the VSS is expressed by:

$$\boldsymbol{\tau}_{vss} = \mathbf{M}_s\ddot{\mathbf{q}}_s + \mathbf{h}_s(\mathbf{q}_s, \dot{\mathbf{q}}_s) + \mathbf{f}_s - \boldsymbol{\tau}_s \tag{8}$$

where $\mathbf{M}_s$ is an $(n \times n)$ definite positive matrix of inertia depending on the variable stiffness joints coordinates $\mathbf{q}_s$, and $\mathbf{h}_s$ is an n-dimensional vector of Coriolis, centrifugal and gravitational effects and its value depends on the variable stiffness joints coordinates $\mathbf{q}_s$ and their time derivatives $\dot{\mathbf{q}}_s$. $\mathbf{f}_s$ is an n-dimensional vector grouping the variable stiffness joint friction terms.

In the next section, we explain how our motion generator exploits the dynamic model (6)–(8) in order to generate energy efficient pick-and-place motions.

3 Exploiting the robot natural dynamics

During an energy-efficient pick-and-place operation, there are two main performances expected to be achieved from the high-speed robot: *i*) to accurately meet the desired boundary conditions (*pick* or *place* positions), and *ii*) to perform the task with minimum energy-demand from the actuators, both expected performances to be completed in a given motion duration. This means that there is no restriction for the robot on how to go from the initial to the final positions, except eventual collisions within the robot links, external environment or singularity loci, as long as it is the most energy-efficient. Indeed, in our work, we consider that we have checked *a priori* that the workspace in which the robot will move is free of collision and singularity free. Managing the presence of singularity or collisions with the external environment and/or between the robot links is left as a future work.

For this, let us exploit the results shown in [28] in which it is shown that more that 90 % of loss for the actuation chain in a typical high-speed pick-and-place operation are due to the resistive and conduction losses which are quadratic functions of the motor electric currents, and thus, of the motor input efforts $\boldsymbol{\tau}$ and $\boldsymbol{\tau}_{vss}$, during the deceleration phase. That is why, based on this previous hypothesis, by imposing $\boldsymbol{\tau}$ and $\boldsymbol{\tau}_{vss}$ to be null during the deceleration phase, we may considerably reduce the energy losses. However, as it will be explained thereafter, these conditions are not achievable, and we are going to propose an alternative based on cancelling the time-derivatives of the input efforts.

As a result, in this section, we propose an algorithm based on a BVP that imposes $\dot{\boldsymbol{\tau}}$ and $\dot{\boldsymbol{\tau}}_{vss}$ to be zero during the robot deceleration phase. The algorithm will be detailed after a short recall on how to solve a BVP based on the shooting method.

3.1 Solution of BVP by using the shooting method

In the field of numerical methods for solving differential equations, a BVP is defined when two conditions are given at different values of the independent variable of the differential equation [34], i.e.:

$$h' = f(t,h), \qquad a < t < b \tag{9}$$

with the boundary conditions:

$$h(a) = P_A, \qquad h(b) = P_B \tag{10}$$

where (9) is a second order differential equation, t is the independent variable, P_A and P_B are the desired boundary conditions at $t = a$ and $t = b$ of the BVP.

The classical way to use the shooting method to solve the BVP (9)-(10) is by treating it as an initial value problem (IVP) [34], in which the initial conditions are given by:

$$h(a) = P_A, \qquad h'(a) = \alpha \tag{11}$$

where α represents the slope of the solution, i.e. the first derivative of $h(t)$ at $t = a$, and it must be chosen in such a way that the solution of (9) satisfies the remaining boundary condition $h(b) = P_B$ from (10).

Thus, in a similar vein, this paper proposes to use a BVP formulation to exploit the natural motions of the pseudo-periodic pick-and-place oscillations of the parallel robot. The algorithm is detailed below.

3.2 BVP applied on energy-efficient high-speed robots

According to the expressions (6) and (8), if $\boldsymbol{\tau}$, $\boldsymbol{\tau}_{vss}$ are null during the deceleration phase starting at a time t_k up to

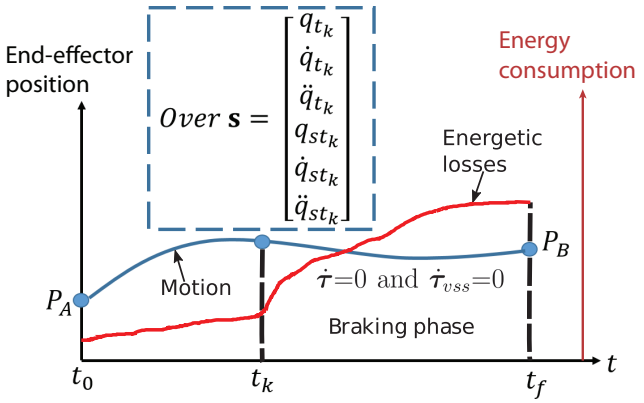

Fig. 3. Graphical interpretation of shooting method for solving the BVP for the robot-plus-VSS system.

the time t_f, then we can find that, for $t \in [t_k, t_f]$:

$$\begin{aligned} \ddot{\mathbf{q}} &= -\mathbf{M}^{-1}(\mathbf{c} + \mathbf{K}(\mathbf{q} - \mathbf{q}_s) + \dot{\mathbf{f}}_a) \\ \ddot{\mathbf{q}}_s &= \mathbf{J}_s^{-1}(\mathbf{K}(\mathbf{q} - \mathbf{q}_s) - \mathbf{f}_s) \end{aligned} \tag{12}$$

with initial boundary conditions $\dot{\mathbf{q}}(t_k) = \dot{\mathbf{q}}_{t_k}$, $\dot{\mathbf{q}}_s(t_k) = \dot{\mathbf{q}}_{st_k}$ and $\mathbf{q}(t_k) = \mathbf{q}_{t_k}$, $\mathbf{q}_s(t_k) = \mathbf{q}_{st_k}$, $\dot{\mathbf{q}}_{t_k}$, $\dot{\mathbf{q}}_{st_k}$, $\mathbf{q}_{t_k}$ and $\mathbf{q}_{st_k}$ being fixed values. With these four initial conditions, we cannot ensure to attain the six final boundaries at time t_f which are: desired motor positions $\mathbf{q}(t_f) = \mathbf{q}^*_{t_f}$, $\mathbf{q}_s(t_f) = \mathbf{q}^*_{st_f}$, desired motor velocities $\dot{\mathbf{q}}(t_f) = \dot{\mathbf{q}}^*_{t_f}$, $\dot{\mathbf{q}}_s(t_f) = \dot{\mathbf{q}}^*_{st_f}$ (usually equal at 0) and desired motor accelerations $\ddot{\mathbf{q}}(t_f) = \ddot{\mathbf{q}}^*_{t_f}$, $\ddot{\mathbf{q}}_s(t_f) = \ddot{\mathbf{q}}^*_{st_f}$ (usually also null). Therefore, the problem needs to be modified.

With the purpose of being able to specify acceleration constraints in the BVP formulation, we will thus time differentiate the dynamic expressions (6) and (8) in order to obtain the jerk equations:

$$\dot{\boldsymbol{\tau}} = \mathbf{M}\dddot{\mathbf{q}} + \dot{\mathbf{M}}\ddot{\mathbf{q}} + \dot{\mathbf{c}} + \mathbf{K}(\dot{\mathbf{q}} - \dot{\mathbf{q}}_s) + \dot{\mathbf{f}}_a \tag{13}$$

$$\dot{\boldsymbol{\tau}}_{vss} = \mathbf{J}_s\dddot{\mathbf{q}}_s - \mathbf{K}(\dot{\mathbf{q}} - \dot{\mathbf{q}}_s) + \dot{\mathbf{f}}_s \tag{14}$$

If, for $t \in [t_k, t_f]$, $\dot{\boldsymbol{\tau}} = 0$ and $\dot{\boldsymbol{\tau}}_{vss} = 0$, then:

$$\dddot{\mathbf{q}} = -\mathbf{M}^{-1}(\dot{\mathbf{M}}\ddot{\mathbf{q}} + \dot{\mathbf{c}} + \mathbf{K}(\dot{\mathbf{q}} - \dot{\mathbf{q}}_s) + \dot{\mathbf{f}}_a) \tag{15}$$

$$\dddot{\mathbf{q}}_s = \mathbf{J}_s^{-1}(\mathbf{K}(\dot{\mathbf{q}} - \dot{\mathbf{q}}_s) - \dot{\mathbf{f}}_s) \tag{16}$$

with initial boundary conditions: $\ddot{\mathbf{q}}(t_k) = \ddot{\mathbf{q}}_{t_k}$, $\ddot{\mathbf{q}}_s(t_k) = \ddot{\mathbf{q}}_{st_k}$, $\dot{\mathbf{q}}(t_k) = \dot{\mathbf{q}}_{t_k}$, $\dot{\mathbf{q}}_s(t_k) = \dot{\mathbf{q}}_{st_k}$ and $\mathbf{q}(t_k) = \mathbf{q}_{t_k}$, $\mathbf{q}_s(t_k) = \mathbf{q}_{st_k}$, $\ddot{\mathbf{q}}_{t_k}$ and $\ddot{\mathbf{q}}_{st_k}$ being fixed values. For these six known initial configurations are t_k, the system of nonlinear ordinary differential equations (ODEs) (15)–(16) can be solved by using a standard Runge-Kutta approach, and a shooting method can be used in order to find the values of these six initial boundary conditions leading to $\mathbf{q}(t_f) = \mathbf{q}^*_{t_f}$, $\mathbf{q}_s(t_f) = \mathbf{q}^*_{st_f}$, $\dot{\mathbf{q}}(t_f) = \dot{\mathbf{q}}^*_{t_f}$, $\dot{\mathbf{q}}_s(t_f) = \dot{\mathbf{q}}^*_{st_f}$, $\ddot{\mathbf{q}}(t_f) = \ddot{\mathbf{q}}^*_{t_f}$ and $\ddot{\mathbf{q}}_s(t_f) = \ddot{\mathbf{q}}^*_{st_f}$. In this work, we used a Runge-Kutta method of order 4.

Obviously, fixing $\dot{\boldsymbol{\tau}} = 0$ and $\dot{\boldsymbol{\tau}}_{vss} = 0$ impose $\boldsymbol{\tau}$ and $\boldsymbol{\tau}_{vss}$ to be constant vectors of input efforts. Nevertheless, we can tune (or optimize) the value of t_k such that the squared norm of $\boldsymbol{\tau}(t) = [\boldsymbol{\tau}^T(t)\ \boldsymbol{\tau}^T_{vss}(t)]^T$ for $t \in [t_k, t_f]$ (or even during the whole motion duration) is as small as possible, thus tending to minimizing the energy consumption. As shown later in Section 4, this heuristic works very well in practice.

These considerations being taken into account, in a given pick-and-place cycle between two points P_A and P_B with given duration t_f (Fig. 3), we recall that most of the energetic losses are accumulated during the braking phase of the high-speed motion. That is why, we can consider the full cycle as two motion segments, i.e. a motion segment from t_0 (initial time when the robot is at P_A) to t_k, and a braking segment from t_k to t_f, in which t_k represents the time at which the braking phase starts. As a result:

- For $t \in [t_k, t_f]$, i.e. on the end of the motion, corresponding essentially to the decelerating phase, the motion will be defined by solving the BVP based on the system of ODEs (15)–(16): thanks to a shooting method, the initial boundary conditions $\mathbf{s} = [\mathbf{q}_{t_k}^T\ \dot{\mathbf{q}}_{t_k}^T\ \ddot{\mathbf{q}}_{t_k}^T\ \mathbf{q}_{st_k}^T\ \dot{\mathbf{q}}_{st_k}^T\ \ddot{\mathbf{q}}_{st_k}^T]^T$ at t_k (Fig. 3) are found such that the final desired motor positions $\mathbf{q}^*_{t_f}$, $\mathbf{q}^*_{st_f}$, velocities $\dot{\mathbf{q}}^*_{t_f}$, $\dot{\mathbf{q}}^*_{st_f}$ and accelerations $\ddot{\mathbf{q}}^*_{t_f}$, $\ddot{\mathbf{q}}^*_{st_f}$ are attained at $t = t_f$.
- Then, for $t \in [t_0, t_k[$, i.e. during the time for which the energetic losses remain without drastic increases, and are less preponderant with respect to the braking phase, a classical $5th$-degree polynomial motion profile is used to create a motion between (i) the motion starting conditions (at time t_0) with desired motor positions $\mathbf{q}(t_0) = \mathbf{q}^*_0$, $\mathbf{q}_s(t_0) = \mathbf{q}^*_{s_0}$, velocities $\dot{\mathbf{q}}(t_0) = \dot{\mathbf{q}}^*_0$, $\dot{\mathbf{q}}_s(t_0) = \dot{\mathbf{q}}^*_{s_0}$ and accelerations $\ddot{\mathbf{q}}(t_0) = \ddot{\mathbf{q}}^*_0$, $\ddot{\mathbf{q}}_s(t_0) = \ddot{\mathbf{q}}^*_{s_0}$, and (ii) the motion conditions at time t_k defined by the vector $\mathbf{s}$ found by solving the previous BVP on $t \in [t_k, t_f]$.

From the previous BVP formulation and from the definition of the decision variable vector $\mathbf{s}$, it should be noted that since there is the same number of final boundary conditions at time t_f as number of decision variables in $\mathbf{s}$, from theory of shooting algorithms in [34], we know that it should be possible to find a solution for such BVP by using the shooting formulation since the optimization problem is squared. It should also be mentioned that for solving the BVP with the shooting method, we used a *Levenberg - Marquardt* (LM) algorithm [35]. The shooting method algorithm is defined in Algorithm 1.

In this algorithm, max_k is the maximum number of iterations, $\boldsymbol{\varepsilon}_{1\ldots6}$ represent error thresholds, RK4 is an ODE solver for (15)-(16) (here, a Runge-Kutta method of order 4) and LMUpdate is a function representing the Levenberg-Marquardt updating law based on [35]. It should be noted that, from the aforementioned algorithm, expressions (15) and (16) are integrated at each iteration in order to evaluate $(\mathbf{E}_q(\mathbf{s}_k), \mathbf{E}_{\dot{q}}(\mathbf{s}_k), \mathbf{E}_{\ddot{q}}(\mathbf{s}_k), \mathbf{E}_{q_s}(\mathbf{s}_k), \mathbf{E}_{\dot{q}_s}(\mathbf{s}_k), \mathbf{E}_{\ddot{q}_s}(\mathbf{s}_k))$, which means that $\mathbf{M}$ from (15) must be numerically invertible, i.e. out of Type 2 singularity [33]. Thus, in the integration step, an inversion-checking condition defined by $|\kappa(\mathbf{q})| < \gamma$, where κ represents the condition of proximity to singularity with γ denoting a threshold, is added to verify the inversion condition. As a condition of proximity to singularity, we compute the condition number of the matrix $\mathbf{A}$ in (1), which is the kinematic matrix that degenerates in the singularity locus, see [36] for an example of this condition. Any other criterion characterizing the proximity to singularity could be

Algorithm 1 : Shooting method applied on robot and VSS jerk equations given the desired boundary conditions.

Input: $k \leftarrow 0, max_k \leftarrow 100$, $t_{int} \leftarrow [t_k, ..., t_f]$, $h > 0$, $\mathbf{s}_0 \leftarrow [1, 1, ..., 1]^T$, $t_f > 0$, $t_k > 0$, $t_k < t_f$,

while $|\mathbf{E}_q| > \boldsymbol{\varepsilon}_1$, $|\mathbf{E}_{\dot{q}}| > \boldsymbol{\varepsilon}_2$, $|\mathbf{E}_{\ddot{q}}| > \boldsymbol{\varepsilon}_3$, $|\mathbf{E}_{q_s}| > \boldsymbol{\varepsilon}_4$, $|\mathbf{E}_{\dot{q}_s}| > \boldsymbol{\varepsilon}_5$, $|\mathbf{E}_{\ddot{q}_s}| > \boldsymbol{\varepsilon}_6$, $k \leq max_k$ **do**

$[\mathbf{q}, \dot{\mathbf{q}}, \ddot{\mathbf{q}}, \mathbf{q}_s, \dot{\mathbf{q}}_s, \ddot{\mathbf{q}}_s]_k = \text{RK4}(t_{int}, \mathbf{s}_k, h, (\dddot{\mathbf{q}}, \dddot{\mathbf{q}}_s))$ ▷ Numerical integration with Runge-Kutta $4th$ order of Eqs. (15)-(16)

$$\mathbf{E}(t_f, \mathbf{s}_k) = \begin{cases} \mathbf{E}_q(\mathbf{s}_k) = \mathbf{q}(t_f, \mathbf{s}_k) - \mathbf{q}^*_{t_f} \\ \mathbf{E}_{\dot{q}}(\mathbf{s}_k) = \dot{\mathbf{q}}(t_f, \mathbf{s}_k) - \dot{\mathbf{q}}^*_{t_f} \\ \mathbf{E}_{\ddot{q}}(\mathbf{s}_k) = \ddot{\mathbf{q}}(t_f, \mathbf{s}_k) - \ddot{\mathbf{q}}^*_{t_f} \\ \mathbf{E}_{q_s}(\mathbf{s}_k) = \mathbf{q}_s(t_f, \mathbf{s}_k) - \mathbf{q}^*_{st_f} \\ \mathbf{E}_{\dot{q}_s}(\mathbf{s}_k) = \dot{\mathbf{q}}_s(t_f, \mathbf{s}_k) - \dot{\mathbf{q}}^*_{st_f} \\ \mathbf{E}_{\ddot{q}_s}(\mathbf{s}_k) = \ddot{\mathbf{q}}_s(t_f, \mathbf{s}_k) - \ddot{\mathbf{q}}^*_{st_f} \end{cases} \quad \triangleright \text{ Residuals}$$

at the final motor configurations, velocities and accelerations

$\mathbf{J}_k = \dfrac{\partial \mathbf{E}(t_f, \mathbf{s}_k)}{\partial \mathbf{s}_k}$ ▷ Gradients of the residuals

$\Delta \mathbf{s}_k = \text{LMUpdate}(\mathbf{s}_k, \mathbf{J}_k)$ ▷Levenberg-Marquardt update

$\mathbf{s}_{k+1} = \mathbf{s}_k + \Delta \mathbf{s}_k$

$k = k + 1$

end while

Output:

if $k < max_k$ **then**

$\mathbf{s}_k$ ▷ initial value conditions for Eqs. (15)-(16) ensuring that $|\mathbf{E}| \leq [\boldsymbol{\varepsilon}_1^T \dots \boldsymbol{\varepsilon}_6^T]^T$

else

The problem must be run again with larger value for max_k

end if

used [37].

It should be finally mentioned that, in practice, the Algorithm 1 may have difficulty to converge if the friction terms $\mathbf{f}_a$ and $\mathbf{f}_s$ in Eqs. (6)–(8) are too big, especially the Coulomb friction terms which are modelled with discontinuous "sign" functions [30][2]. In such a case, it is better to remove the friction functions and their time derivatives from the model, and to solve it without them, at the price of a lower energy efficiency.

In order to validate the aforementioned theoretical formulations, the following Section presents experimental results from testing the energy-efficient motion generator on a planar five-bar mechanism with VSS in parallel to the actuated links.

[2]Discontinuous "sign" functions may be approximated by continously differentiable function like "atan" or "tanh", but the slope around 0 may be still very high, leading to potential numerical issues when solving the BVP.

4 Case study: Five-bar mechanism with variable stiffness springs

4.1 Description of the architecture

Here, the description of the full experimental system, i.e. robot and VSS, will be presented, firstly for the five-bar mechanism and then for the variable stiffness system. A five-bar mechanism is a planar parallel robot whose schematic is shown in Fig. 4. This robot is a 2-DOF parallel robot able to perform two translations in the plane (O, $\mathbf{x}_0$, $\mathbf{y}_0$), and which is composed of two legs:

- A first leg composed of 3 revolute joints whose axes are parallel, directed along $\mathbf{z}_0$ and located at points A_{11}, A_{12} and A_{13}, the joint located at point A_{11} being actuated, and
- A second leg composed of 2 revolute joints whose axes are parallel, directed along $\mathbf{z}_0$ and located at points A_{21} and A_{22}, the joint located at point A_{21} being actuated.

All other joints are passive (A_{12}, A_{22}, A_{13}). The actuation of the parallel robot is provided by $\mathbf{q} = [q_{11}, q_{21}]^T$. The vector of moving platform pose is given by $\mathbf{x} = [x, y]^T$. a is the distance between the actuated joints. Finally, ℓ_1 and ℓ_2 represent the length of the proximal links of the robot, and ℓ_3 and ℓ_4 represent the length of the distal links of the robot.

For the design of the five-bar mechanism, the two serial kinematic chains that constitute the parallel robot are of equivalent dimensions and manufactured in aluminum. According to the CAD model for prototyping the five-mechanism in Fig. 5, the robot is thus composed as follows:

- two motors $\mathcal{M}_1$ and $\mathcal{M}_2$ for the actuation of the active joints separated one from each other by a distance of a = 250 mm;
- two proximal links (actuated links) of dimension equal to $\ell_1 = \ell_2$ = 280 mm, and two distal links of dimension equal to $\ell_3 = \ell_4$ = 400 mm;
- the rectangular workspace from Fig. 5 represents the operational workspace for the five-bar prototype.

For the variable stiffness system, the design and functioning principle of the VSS are shown in Fig. 6 for one of the actuated links of the parallel manipulator. Based on Fig. 6, the link-plus-VSS system of each proximal link of the five-bar mechanism is driven by motors ① and ⑧, each of them used for actuating the VSS system (②, ③, ④, ⑤, ⑥) and the robot link ⑦, respectively. As shown in Fig. 6, the deformation of the spring ⑥, and therefore the VSS stiffness, can be adjusted by means of two spring anchor points ($\mathcal{A}_1$ and $\mathcal{A}_2$), each of them controlled by a pulley-belt-transmission system (③, ④, ⑤) on the top, associated to variable q_{s_i}, and by the active joint ⑧ of the robot link on the bottom, associated to the variable q_{i1}. The pulley-belt-transmission system consists of a driving pulley ③, whose displacement is parameterized by q_{s_i}, which transmits the one-to-one ratio to the driven pulley ⑤ connected to the torsional spring ⑥ in parallel with the robot link ⑦. The real five-bar mechanism with VSS in parallel is shown in Fig. 7.

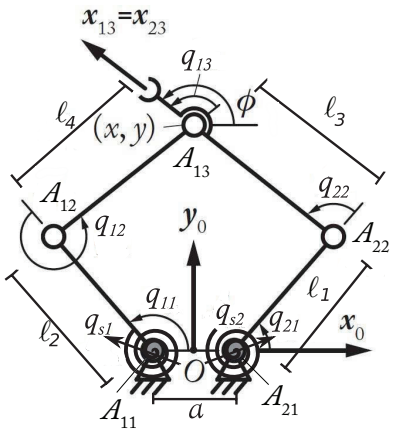

Fig. 4. Five-bar mechanism parameterization with two actuated joints q_{11} and q_{21}, and three passive joints q_{12}, q_{22} and q_{13}. The variable stiffness torsional springs are located in parallel to the two actuated joints defined by q_{s1} and q_{s2}.

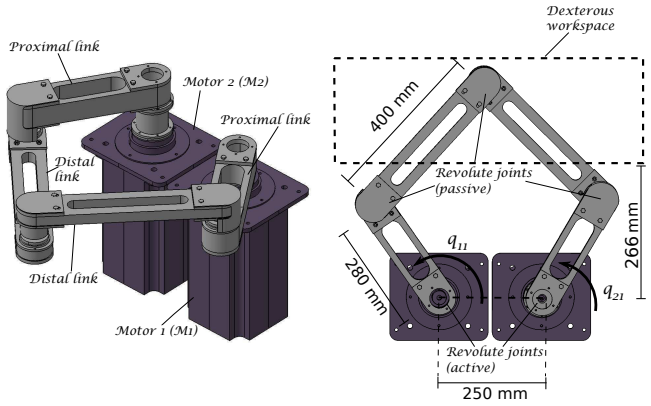

Fig. 5. CAD of five-bar mechanism.

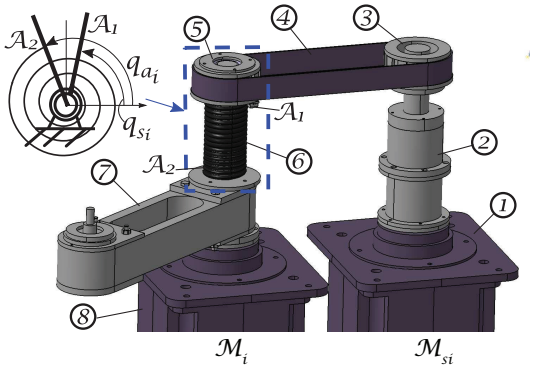

Fig. 6. CAD of variable stiffness system. Numbers in the picture correspond to the main parts of the prototype.

4.2 Dynamic model and identification

The dynamic model of the five-bar mechanism with VSS was computed according to the methodology from Section 2. For the identification of the dynamic parameters of the experimental prototype, a least square method from [38] was used. The resulted identified dynamic model that describes the experimental system is thus given by:

$$\boldsymbol{\tau} = \boldsymbol{\tau}_{ta} - \mathbf{B}^T\boldsymbol{\lambda} + \boldsymbol{\tau}_s, \qquad \mathbf{w}_p = \mathbf{A}^T\boldsymbol{\lambda}, \qquad \boldsymbol{\tau}_{vss} = \mathbf{J}_s - \boldsymbol{\tau}_s \quad (17)$$

with

$$\boldsymbol{\tau}_{ta} = \begin{bmatrix} zz_{11R}\ddot{q}_{11} \\ zz_{21R}\ddot{q}_{21} \end{bmatrix} + \begin{bmatrix} f_{s_1}\text{sign}(\dot{q}_{11}) \\ f_{s_2}\text{sign}(\dot{q}_{21}) \end{bmatrix}, \mathbf{w}_p = m_R \begin{bmatrix} \ddot{x} \\ \ddot{y} \end{bmatrix} \quad (18)$$

$$\boldsymbol{\tau}_s = \begin{bmatrix} k_{11}(q_{11} - q_{s_1}) \\ k_{21}(q_{21} - q_{s_2}) \end{bmatrix} \quad (19)$$

$$\mathbf{J}_s = \begin{bmatrix} J_1\ddot{q}_{s_1} \\ J_2\ddot{q}_{s_2} \end{bmatrix} + \begin{bmatrix} f_{vss_1}\text{sign}(\dot{q}_{s_1}) \\ f_{vss_2}\text{sign}(\dot{q}_{s_2}) \end{bmatrix} + \begin{bmatrix} f_{v_1}(\dot{q}_{s_1}) \\ f_{v_2}(\dot{q}_{s_2}) \end{bmatrix} \quad (20)$$

where:

- m_R is the mass of the end-effector (point A_{13}); m_R = 2.6370 ± 0.08 kg;
- zz_{11R} and zz_{21R} are the grouped inertial effects due to rotation of the mechanism, respectively at the first active joint (A_{11}) and at the second active joints (A_{21}); zz_{11R} = 0.1860 ± $8{\cdot}10^{-3}$ kg.m^2 and zz_{21R} = 0.1805 ± $7{\cdot}10^{-3}$ kg.m^2;
- f_{s_1} is the term of static friction (Coulomb) in the first active joint (respectively f_{s_2} for the second active joint); f_{s_1} = 1.0778 ± 0.1446 Nm and f_{s_2} = 1.2283 ± 0.1267 Nm;
- k_{11} and k_{21} represent the spring constants, respectively for each VSS; k_{11} = 4.6707 ± 0.2297 Nm/rad and k_{21} = 4.4789 ± 0.1595 Nm/rad;
- J_1 and J_2 are the grouped inertial effects due to rotational motion of the variable stiffness system, respectively for the VSS placed in parallel of each actuated link; J_1 = 0.0223 ± $1{\cdot}10^{-3}$ kg.m^2 and J_2 = 0.0122 ± $7{\cdot}10^{-4}$ kg.m^2;
- f_{vss_1} is the term of static friction (Coulomb) grouping the friction effects due to bearings, pulley-belt transmission tension and the friction due to the internal contact of the torsional spring coils (respectively f_{vss_2} for the second VSS); f_{vss_1} = 2.1390 ± 0.1535 Nm and f_{vss_2} = 2.5677 ± 0.1726 Nm;
- f_{v_1} is the term of viscous friction for the motor M_{s_1} of first VSS (respectively f_{v_2} for the motor M_{s_2} of the second VSS); f_{v_1} = 0.0764 ± 0.011 Nms and f_{v_2} = 0.0742

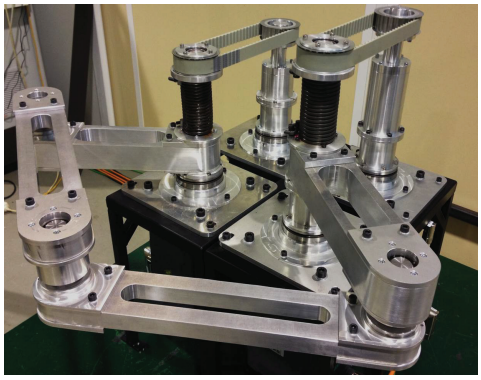

Fig. 7. Real prototype in isometric view.

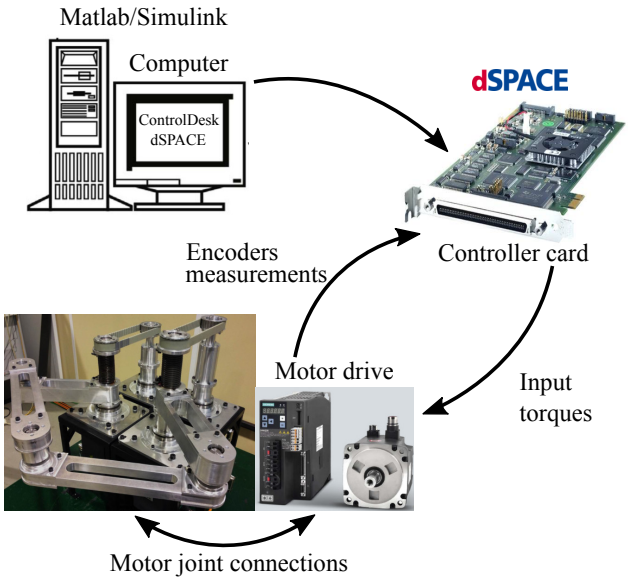

Fig. 8. Experimental benchmark.

$\pm$ 0.023 Nms.

Note that error of estimation provided with the identified parameters is a direct result of the least square identification technique [38].

4.3 Controller design

For controlling the four active joints of the experimental robot, i.e. the two joints from the parallel robot and the two joints from the motors that adjust the equilibrium position of the VSS, a dSPACE controller board was used according to the experimental benchmark shown in Fig. 8. This control card allows to implement real-time control in combination with Matlab/Simulink. Additionally, a Computed Torque Control (CTC) [31] was implemented for tracking the energy-efficient motions computed from the BVP for the five-bar-plus-VSS active joints, i.e. $\mathbf{q} = [q_{11}, q_{21}]$ and $\mathbf{q}_s = [q_{s_1}, q_{s_2}]$, respectively. The CTC is an advanced control technique which computes the input torques that the actuators must apply to the robot in order to track a given trajectory [31]. In this case, the CTC is implemented in order to track as best as possible the motions generated from the BVP, so that the robot-plus-VSS can move as energy-efficient as possible. The bandwidth of the CTC was set at around 12 rad/s.

4.4 Experimental results for reducing energy consumption

In order to validate the theoretical formulations for performing energy-efficient motions, here, we define two sets of desired pick-and-place conditions for testing the energy-efficient motion generator developed in Section 3. It is worth mentioning that, in what follows, for computing the energetic losses for the two experimental scenarios, we estimate the losses thanks to the model presented in [28] that is not recalled here for reasons of brevity. This is because, due to technological limitations, we cannot have a direct measure of the motor energy consumption. In this model, several types of energy losses are taken into account:

- Losses in the motor phases (our actuators are three-phase motors developing a peak torque of 24 Nm for a current of 12.6 A)
- Losses due to a resistance for achieving motor braking
- Conduction and switching losses in the different motor phases due to transistors and diodes
- Rectification losses

Note that, in this model, the losses are quadratic with the intensity of the current circulating in the different motor phases and are linear with the resistances all along the current circuit.

4.4.1 First pick-and-place task

The first set of boundary constraints represents a trajectory symmetrically defined in the operational workspace of the five-bar mechanism (Fig. 9) in which each pick-and-place point is required to be joined at different travel time, and the desired positions are defined as follows:

- $A = [0, 0.4]$, $B = [0.15, 0.38]$, $C = [-0.15, 0.38]$, $D = [0.15, 0.42]$, $E = [-0.15, 0.42]$.

The connecting times for the desired pick-and-place positions are defined respectively in Fig. 9. In order to analyze the results in terms of input torque reduction and energy consumption, two different types of actuation modes were considered: *i*) nominal actuation in which the pick-and-place positions are joined thanks to a classical fifth-degree polynomial and there is no elastic element attached to the actuated links (VSS were dismounted), *ii*) actuation with VSS in parallel of each actuated link and in which the trajectories are generated thanks to the BVP formalized in Section 3.

Here, it should be mentioned that for the nominal actuation case (without VSS), the robot was not able to track the desired trajectory in Fig. 9. This is because, for the nominal actuation case, this trajectory is dynamics demanding and it requires to develop motor torques higher than the motor limit torques (23.9 Nm). Therefore, the results presented below for the nominal type of actuation for the test trajectories were computed in simulation. Note that we used the model of the nominal actuation case because it was properly identified using the method [38], leading to a motor torque prediction with less than 5 % of error. We did not meet this issue for the actuation case when using VSS: for this, real experimental results are provided. We recorded the reference torques sent by the controller to the motors, which can be considered as the real torques developed by the motors due to the very high bandwidth of the motor current loop.

For the set of boundary positions shown in Fig. 9, the RMS values of the input torques from the full actuation chain are grouped in Table 1. It can be seen that the reduction of torques RMS between the nominal and VSS actuation cases is about 70 %. In addition to the aforementioned results in terms of input torques reduction, in the last column of Ta-

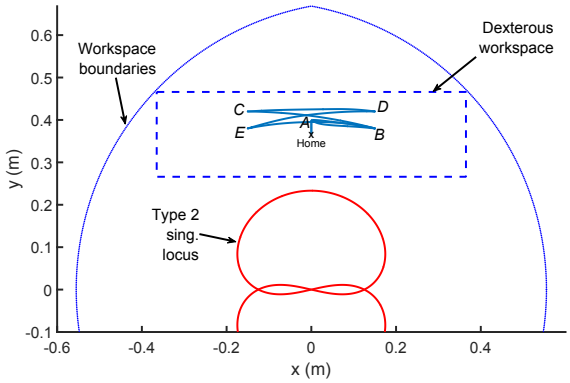

Fig. 9. Multiple-point pick-and-place sequence in the five-bar mechanism workspace: $A \rightarrow B$ (travel time: 0.32 s), $B \rightarrow C$ (travel time: 0.31 s), $C \rightarrow D$ (travel time: 0.30 s), $D \rightarrow E$ (travel time: 0.31 s), $E \rightarrow B$ (travel time: 0.34 s), $B \rightarrow A$ (travel time: 0.31 s).

ble 1, we compare the RMS of the torques delivered by each of the motor in the nominal actuation case to the RMS of the vector $\|\tau_i \, \tau_{vss_i}\|$ ($i = 1,2$, τ_i being the torque of motor $\mathcal{M}_i$, τ_{vss_i} being the torque delivered to move the VSS associated with motor $\mathcal{M}_i$). These RMS values are directly related to the energy consumption of the full actuation chain for each motorized link and will used as a substitution metrics of the energy consumption that cannot be directly measured in our benchmark, as previously explained. It can thus be seen in Table 1, the input torque RMS reduction can reach up to 54 % when considering the full actuation chains.

The results in terms of energetic losses from the two types of actuation (nominal and by using VSS) are shown in Fig. 10. First of all, it should be noted that during the evolution of the energetic losses along the motion for the case of nominal actuation, most of the losses appears during the braking phase. This can be seen thanks to all the increments appearing in the deceleration phase when the robot approaches all the *place* positions. That is why, thanks to the solution of the BVP, to exploit the natural dynamics during the braking phase, the energetic losses from the full actuation chain can be drastically reduced by 55 %. This can be seen during all the braking phases along the evolution of the losses for the case when using VSS, in which the energetic losses are drastically reduced with respect to the nominal case, leading to a remarkable percentage of energy savings. It should be also noted that based on Fig. 11, while being able to ensure energy-efficient motions, putting VSS in parallel with the actuated links (and not in series, as if we were using VSA), the tracking error along the desired pick-and-place motion remains bounded on the order of 10^{-3} rad, which is rather small.

4.4.2 Second pick-and-place task

For the second set of boundary constraints, the required pick-and-place task to be performed follows from an asymmetric shape as it can be seen in Fig. 12. The pick-and-place desired positions must be joined at variable times defined in

Table 1. RMS values of input torques for nominal case and for case when using VSS in parallel for first pick-and-place task.

Nominal RMS. Torques	Using VSS in parallel RMS. Torques		
$\boldsymbol{\tau}_{\text{RMS}}$ (Nm)	$\boldsymbol{\tau}_{\text{RMS}}$ (Nm)	$\boldsymbol{\tau}_{vss_{\text{RMS}}}$ (Nm)	$[\tau_i \, \tau_{vss_i}]_{\text{RMS}}$ $(i = 1,2)$ (Nm)
[12.84, 13.62]	[3.12, 3.18]	[2.70, 4.28]	[4.64, 6.40]

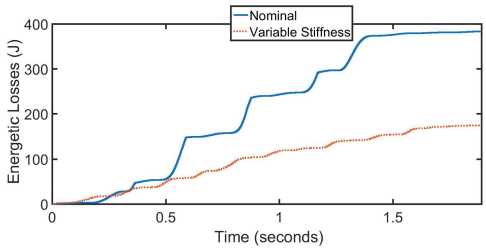

Fig. 10. Comparison of energetic losses for two types of actuation: nominal and case when using VSS for first pick-and-place task.

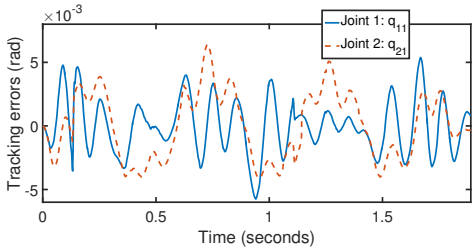

Fig. 11. Tracking errors along the trajectory generated for the first set of boundary pick-and-place conditions.

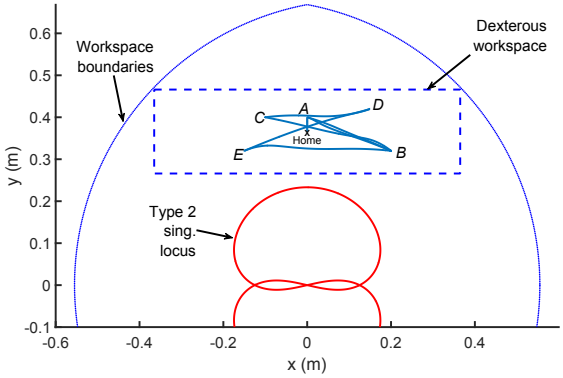

Fig. 12. Multiple-point pick-and-place sequence in the five-bar mechanism workspace: $A \rightarrow B$ (travel time: 0.33 s), $B \rightarrow C$ (travel time: 0.32 s), $C \rightarrow D$ (travel time: 0.32 s), $D \rightarrow E$ (travel time: 0.31 s), $E \rightarrow B$ (travel time: 0.33 s), $B \rightarrow A$ (travel time: 0.31 s).

Fig. 12, with boundary conditions defined here:

- $A = [0, 0.4]$, $B = [0.2, 0.32]$, $C = [-0.1, 0.4]$, $D = [0.15, 0.42]$, $E = [-0.15, 0.32]$.

Table 2. RMS values of input torques distribution for nominal case and for case when using VSS in parallel for second pick-and-place task.

Nominal RMS. Torques	Using VSS in parallel RMS. Sum of Torques
$\boldsymbol{\tau}_{\text{RMS}}$ (Nm)	$[\tau_i \, \tau_{vss_i}]_{\text{RMS}}$ $(i = 1,2)$ (Nm)
[14.38, 13.17]	[5.56, 7.40]

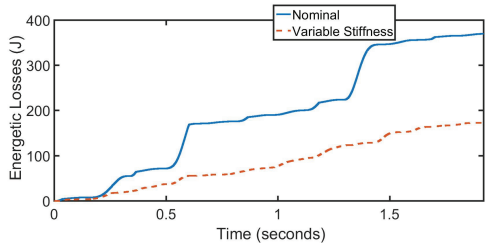

Fig. 13. Comparison of energetic losses for two types of actuation: nominal and case when using VSS for second pick-and-place task.

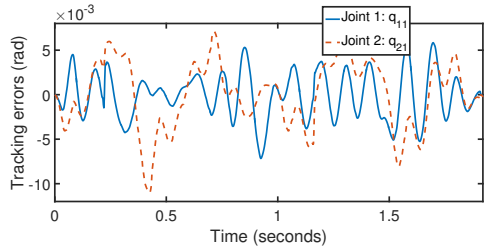

Fig. 14. Tracking errors along the trajectory generated for the second set of boundary pick-and-place conditions.

In Table 2, the robot plus VSS input torques RMS are compared with respect to the nominal type of actuation. The results show that thanks to the distribution of efforts in the energy-efficient actuation, based on Table 2, it can be seen that the input torque reduction can reach up to 44 %. The results in terms of reduction of the energetic losses from the two types of actuation (nominal and by using VSS) are shown in Fig. 13. It can be seen that the energetic losses from the full actuation chain when considering the friction losses in Fig. 13 can be drastically reduced by a 54 %. Finally, Fig. 14 shows a tracking error on the order of 10^{-3}, from the CTC performed along the desired pick-and-place motion, which still confirm the possibility to have a great positioning accuracy of the system composed of the robot plus the VSS.

All these results confirm the interest of the approach for decreasing the energy consumption of high-speed robots. Note that, in [39], the same approach was successfully applied in simulation to a 3-degrees-of-freedom DELTA robot with randomized via points distributed in the workspace, showing the versatility of the approach.

5 Conclusions

This paper proposes a strategy to perform energy-efficient high-speed pick-and-place motions by placing VSS in parallel to the actuated links of high-speed robots, and combining it with a proper motion generator. This motion generator was based on solving a boundary value problem (BVP), in which the objective was to exploit the combined motion of the robot active joints and VSS joints for minimizing the energy consumption. By exploiting this actuation property, we were able to minimize the robot and VSS input torques simultaneously, and thus the full actuation chain energy consumption for fast quasi-periodic motions. Experimental results of the suggested approach on a five-bar mechanism with VSS in parallel to the actuated links showed the drastic reduction of energy consumption of around 55 % on pick-and-place trajectories. These energy consumption reduction results did not neglect the energy required to actuate VSS, contrary to previous existing works.

Future works on this subject includes the development of a strategy to generate energy-efficient motions in case the dynamic parameters are not previously identified, thus considering uncertainties on the dynamic model. We are also going to consider the case of variable end-effector payload in each segment of the pick-and-place task.

Acknowledgements

This work was conducted with the support of the Mexican Council for Science and Technology (CONACYT).

References

[1] Brossog, M., Bornschlegl, M., and Franke, J., 2015. "Reducing the energy consumption of industrial robots in manufacturing systems". International Journal of Advanced Manufacturing Technology, **78**(5–8), pp. 1315–1328.

[2] Briot, S., Caro, S., and Germain, C., 2017. "Design Procedure for a Fast and Accurate Parallel Manipulator". Journal of Mechanisms and Robotics, **9**(6), 10.

[3] Carabin, G., Wehrle, E., and Vidoni, R., 2017. "A review on energy-saving optimization methods for robotic and automatic systems". Robotics, **6**(4), p. 39.

[4] Vidussi, F., Boscariol, P., Scalera, L., and Gasparetto, A., 2021. "Local and Trajectory-Based Indexes for Task-Related Energetic Performance Optimization of Robotic Manipulators". Journal of Mechanisms and Robotics, **13**(2), 03.

[5] Kim, Y., 2017. "Anthropomorphic low-inertia high-stiffness manipulator for high-speed safe interaction". IEEE Transactions on Robotics, **33**(6), pp. 1358–1374.

[6] Arakelian, V., Dahan, M., and Smith, M., 2000. "A historical review of the evolution of the theory on balancing of mechanisms". In Proceedings of the HMM2000 International Symposium on History of Machines and Mechanisms, pp. 291–300.

[7] Baradat, C., Arakelian, V., Briot, S., and Guégan, S., 2008. "Design and prototyping of a new balancing mechanism for spatial parallel manipulators". ASME

Journal of Mechanical Design, **130**(7), pp. 072305–1–072305–13.

[8] Chu, Y.-L., and Kuo, C.-H., 2017. "A Single-Degree-of-Freedom Self-Regulated Gravity Balancer for Adjustable Payload1". Journal of Mechanisms and Robotics, **9**(2), 03.

[9] Pratt, G., and Williamson, M., 1995. "Series elastic actuators". In Proceedings of the 1995 IEEE/RSJ International Conference on Intelligent Robots and Systems. Human Robot Interaction and Cooperative Robots, Vol. 1, pp. 399–406.

[10] Van Ham, R., Thomas, S., Vanderborght, B., Hollander, K., and Lefeber, D., 2009. "Compliant actuator designs: review of actuators with passive adjustable compliance/controllable stiffness for robotic applications". IEEE Robotics and Automation Magazine, **16**(3), pp. 81–94.

[11] Wolf, S., Grioli, G., Eiberg, O., Friedl, W., Grebenstein, M., Catalano, M., Lefeber, D., Stramigioli, S., Tsagarakis, N., Van Damme, M., Van Ham, R., Vanderborght, B., Visser, L., Bicchi, A., and Albu-Schaeffer, A., 2016.. "Variable stiffness actuators: Review on design and components". IEEE/ASME Transactions on Mechatronics, **21**(5), pp. 2418–2430.

[12] Ning, Y., Huang, H., Xu, W., Zhang, W., and Li, B., 2021. "Design and Implementation of a Novel Variable Stiffness Actuator With Cam-Based Relocation Mechanism". Journal of Mechanisms and Robotics, **13**(2), 01.

[13] Stücheli, M., Daners, M. S., and Meboldt, M., 2017. "Benchmark of the Compactness Potential of Adjustable Stiffness Mechanisms". Journal of Mechanisms and Robotics, **9**(5), 08.

[14] Mathijssen, G., Lefeber, D., and Vanderborght, B., 2015. "Variable recruitment of parallel elastic elements: Series parallel elastic actuators (spea) with dephased mutilated gears". IEEE/ASME Transactions on Mechatronics, **20**(2), pp. 594–602.

[15] Furnémont, R., Mathijssen, G., Verstraten, T., Lefeber, D., and Vanderborght, B., 2016. "Bi-directional series-parallel elastic actuator and overlap of the actuation layers". Bioinspiration & biomimetics, **11**(1), pp. 1–18.

[16] Pratt, J., Chee, M., Torres, A., Dilworth, P., and Pratt, G., 2001. "Virtual model control: an intuitive approach for bipedal locomotion". The International Journal of Robotics Research, **20**(2), pp. 129–143.

[17] Tsagarakis, N., Laffranchi, M., Vanderborght, B., and Caldwell, D., 2009. "A compact soft actuator unit for small scale human friendly robots". In Proceedings of the 2009 IEEE International Conference on Robotics and Automation (ICRA 2009), pp. 4356–4362.

[18] Jafari, A., Tsagarakis, N., and Caldwell, D., 2011. "Exploiting natural dynamics for energy minimization using an actuator with adjustable stiffness (awas)". In Proceedings of 2011 IEEE I IEEE International Conference on Robotics and Automation (ICRA 2011), pp. 4632–4637.

[19] Barreto, J., Schöler, F., and Corves, B., 2016. The concept of natural motion for pick and place operations. Mechanisms and Machine Science. Springer, Cham, pp. 89–98.

[20] Schiehlen, W., and Guse, N., 2005. "Control of limit cycle oscillations". In Proceedings of the IUTAM Symposium on Chaotic Dynamics and Control of Systems and Processes in Mechanics, pp. 429–439.

[21] Scalera, L., Carabin, G., Vidoni, R., and Wongratanaphisan, T. "Energy efficiency in a 4-dof parallel robot featuring compliant elements". International Journal of Mechanics and Control, **20**.

[22] van der Spaa, L. F., Wolfslag, W. J., and Wisse, M., 2019. "Unparameterized optimization of the spring characteristic of parallel elastic actuators". IEEE Robotics and Automation Letters, **4**(2), pp. 854–861.

[23] Santina, C. D., and Albu-Schaeffer, A., 2021. "Exciting efficient oscillations in nonlinear mechanical systems through eigenmanifold stabilization". IEEE Control Systems Letters, **5**(6), pp. 1916–1921.

[24] Carabin, G., Scalera, L., Wongratanaphisan, T., and Vidoni, R., 2021. "An energy-efficient approach for 3d printing with a linear delta robot equipped with optimal springs". Robotics and Computer-Integrated Manufacturing, **67**, p. 102045.

[25] Uemura, M., and Kawamura, S., 2009. "Resonance-based motion control method for multi-joint robot through combining stiffness adaptation and iterative learning control". In Proceedings of 2009 IEEE International Conference on Robotics and Automation (ICRA 2009), pp. 1543–1548.

[26] Goya, H., Matsusaka, K., Uemura, M., Nishioka, Y., and Kawamura, S., Proceedings of the 2012 IEEE/RSJ International Conference on Intelligent Robots and Systems (IROS 2012). "Realization of high-energy efficient pick-and-place tasks of scara robots by resonance". In 2012, pp. 2730–2735.

[27] Hollander, K., and Sugar, T., 2004. "Concepts for compliant actuation in wearable robotic systems". In Proceedings of the US-Korea Conference on Science, Technology and Entrepreneurship (UKC 04), Vol. 128, pp. 644–650.

[28] Balderas Hill, R., Briot, S., Chriette, A., and Martinet, P., 2018. "Increasing energy efficiency of high-speed parallel robots by using variable stiffness springs and optimal motion generation". In Proceedings of the ASME 2018 International Design Engineering Technical Conferences & Computers and Information in Engineering Conference (IDETC/CIE 2018).

[29] Balderas-Hill, R., Briot, S., Chriette, A., and Martinet, P., 2018. "Minimizing input torques of a high-speed five-bar mechanism by using variable stiffness springs". In Proceedings of the 22nd CISM IFToMM Symposium on Robot Design, Dynamics and Control (RoManSy 2018).

[30] Briot, S., and Khalil, W., 2015. Dynamics of Parallel Robots – From Rigid Links to Flexible Elements. Springer.

[31] Khalil, W., and Dombre, E., 2004. Modeling, identification and control of robots. Hermès.
[32] Merlet, J., 2006. Parallel Robots. Springer.
[33] Gosselin, C., and Angeles, J., 1990. "Singularity analysis of closed-loop kinematic chains". IEEE Transactions on Robotics and Automation, **6**(3), pp. 281–290.
[34] Roberts, S., and Shipman, J., 1972. Two-Point Boundary Value Problems: Shooting Methods. Elsevier, New-York.
[35] Moré, J., 1978. The Levenberg-Marquardt algorithm: Implementation and theory, Vol. 630 of Numerical Analysis. Lecture Notes in Mathematics. Springer.
[36] Balderas Hill, R., Six, D., Chriette, A., Briot, S., and Martinet, P., 2017-05. "Crossing type 2 singularities of parallel robots without pre-planned trajectory with a virtual-constraint-based controller". In Proceedings of 2017 IEEE International Conference on Robotics and Automation (ICRA 2017).
[37] Merlet, J., 2006. "Jacobian, manipulability, condition number, and accuracy of parallel robots". ASME Journal of Mechanical Design, **128**(1), pp. 199–206.
[38] Hollerbach, J., Khalil, W., and Gautier, M., 2008. Model Identification. Springer, London, ch. 14.
[39] Balderas Hill, R., Briot, S., Chriette, A., and Martinet, P. "Minimizing the energy consumption of a delta robot by exploiting the natural dynamics". In Proceedings of the 23rd CISM IFToMM Symposium on Robot Design, Dynamics and Control (RoManSy 2020).